Langmuir

Article

pubs.acs.org/Langmuir

Effects of Fluid Shear Stress on Polyelectrolyte Multilayers by Neutron Scattering Studies

Saurabh Singh,[†] Ann Junghans,[†] Erik Watkins,[†] Yash Kapoor,[‡] Ryan Toomey,[§] and Jaroslaw Majewski*[,†]

[†]MPA/CINT/Manual Lujan Jr. Neutron Scattering Center, Los Alamos National Laboratory, Los Alamos, New Mexico 87545, United States

[‡]Vision Care R&D, Alcon, Johns Creek, Georgia 30097, United States

[§]Department of Chemical & Biomedical Engineering, University of South Florida, Tampa, Florida 33620, United States

Supporting Information

ABSTRACT: The structure of layer-by-layer (LbL) deposited nanofilm coatings consists of alternating polyethylenimine (PEI) and polystyrenesulfonate (PSS) films deposited on a single crystal quartz substrate. LbL-deposited nanofilms were investigated by neutron reflectomery (NR) in contact with water in the static and fluid shear stress conditions. The fluid shear stress was applied through a laminar flow of the liquid parallel to the quartz/polymer interface in a custom-built solid−liquid interface cell. The scattering length density profiles obtained from NR results of these polyelectrolyte multilayers (PEM), measured under different shear conditions, showed proportional decrease of volume fraction of water hydrating the polymers. For the highest shear rate applied (ca. 6800 s^{-1}) the water volume fraction decreased by approximately 7%. The decrease of the volume fraction of water was homogeneous through the thickness of the film. Since there were not any significant changes in the total polymer thickness, it resulted in negative osmotic pressures in the film. The PEM films were compared with the behavior of thin films of thermoresponsive poly(*N*-isopropylacrylamide) (pNIPAM) deposited via spin-coating. The PEM and pNIPAM differ in their interactions with water molecules, and they showed opposite behaviors under the fluid shear stress. In both cases the polymer hydration was reversible upon the restoration of static conditions. A theoretical explanation is given to explain this difference in the effect of shear on hydration of polymeric thin films.

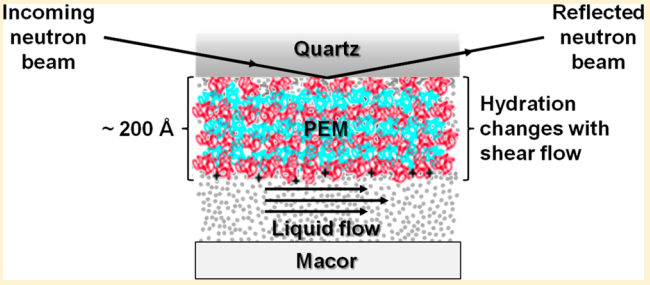

1. INTRODUCTION

Thin films created using a layer-by-layer (LbL) deposition technique are of extraordinary interest with respect to both applications (e.g., catalysis, water purification, electronic or optical devices, sensors, surface coatings, etc.) and basic research in material and life sciences.[1] After the suggestive report by Iler,[2] the LbL assembly of polyions was first realized by Decher and co-workers.[3] The LbL self-assembly technique enables the fabrication of ultrathin films by a sequential deposition driven by electrostatic interactions of charged polymers, nanoparticles, biological templates, or biologically active species.[3] An inherently charged substrate is consecutively exposed to solutions of oppositely charged species, which adsorb to the developing film at rates that enable nanometer-scale control of film thickness.

In the field of implantable biomaterials and tissue engineered constructs, surface properties are of high importance as they have an influence on subsequent tissue and cellular events such as protein adsorption, cell adhesion, and inflammatory response, all of these events being necessary for tissue remodeling.[4] It is well recognized that implantable medical devices are becoming increasingly important in the practice of modern medicine. The possibility of creating composite nanostructures—by combining different polyions, nanoparticles, enzymes, proteins, and DNAs—extends the number of applications where such thin films can be used. LbL-deposited thin films can be made biocompatible by terminating the outermost layer with a stealth polymer such as poly(ethylene glycol) (PEG).[5] Furthermore, these techniques have been found to be of interest in nonimplantable biomaterials such as contact lenses where a nonwetting surface can be rendered hydrophilic for patient comfort.[6] The facile deposition of such nanofilms, the ability to control the thickness with nanometer precision, and the possibility of tailoring the surface properties (e.g., wettability, surface charge, roughness, etc.) make such films highly attractive for biomedical and other applications. For example, dermally implanted luminescent sensors have been proposed for the monitoring of glucose level in diabetics.[7] For faster response, it is proposed that such sensors can be implanted in the close proximity of the blood capillaries in the dermis, which will allow a quick transport of analytes (e.g., glucose) to the sensors. In this situation, the sensors coated

Received: January 9, 2015
Revised: February 14, 2015
Published: February 17, 2015

DOI: 10.1021/acs.langmuir.5b00037
Langmuir 2015, 31, 2870−2878

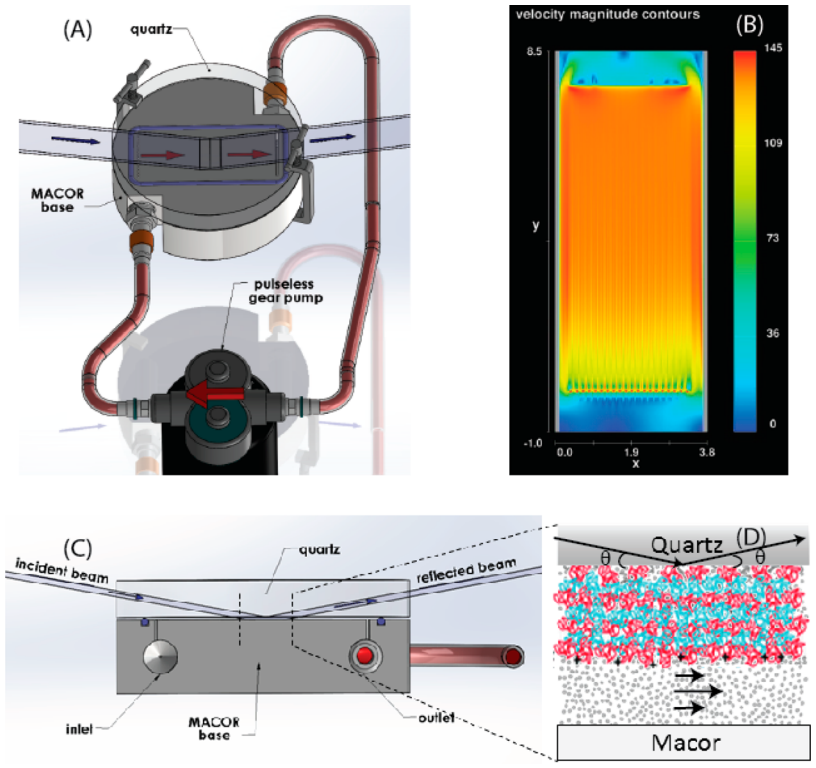

Figure 1. Schematic of the solid−liquid interface cell used in NR experiments. (A) Top and (C) side view of flow cell used. (B) Velocity magnitude contours (cm/s) simulation of the flow halfway between the quartz and the Macor using hydrodynamic code based on Navier−Stokes equations and the geometry of the cell (FLOW-3D, Flow Science, Inc.).[13] This simulation represents laminar flow with Reynolds number of 362; the height of the channel is 0.5 mm, fluid viscosity taken as 0.01 P, and its density as 1 g/cm^3. (D) Schematic of polyelectrolyte multilayer (PEM) adhered to quartz. After layer-by-layer formation of the PEM, the quartz substrate was clamped against a Macor disk with a 0.2−0.3 mm thick, subphase-filled gap created by an O-ring. The D_2O subphase was circulated through the gap by means of a pulse-less gear pump. The neutron beam penetrates the lateral face of the quartz substrate and is scattered from the solid−liquid interface. The solid−liquid interface liquid shear cell was designed following the scheme presented previously.[14]

with nanofilms will also experience fluidic shear from the blood flow. Likewise, biomedical devices such as polymer-coated stents are widely used in modern medicine to repair or replace various elements of the cardiovascular system.[8] Therefore, the ability to estimate the damages/changes induced by shear stresses within such devices is critical for the design optimization process.

To the best of our knowledge, the effect of fluidic shear on the hydration of thin film deposited using the LbL technique has not been investigated hitherto. The shear rates in the human body are in the order of ∼100 s^{-1} in large veins to ∼1500 s^{-1} in capillaries and arterioles.[9] In contrast, ocular shear rates range from 5000 to 28 000 s^{-1} dependent on the thickness of tear film (3−40 μm) and the blink velocity (∼20 cm/s).[10−12] Here, we have studied the effect of fluidic shear on such thin films via neutron reflectometry (NR). Our model system for a LbL-deposited nanofilm coating consisted of polyelectrolyte multilayer deposited from the alternate deposition of polyethylenimine (PEI) and polystyrenesulfonate (PSS) on a 4 in. diameter single crystal quartz substrate. Samples were mounted in a flow cell for which a schematic is shown in Figure 1.

2. EXPERIMENTAL SECTION

2.1. Materials. Branched PEI (50% w/v in H_2O) with a molecular weight of 750 kDa, PSS (powder form) of molecular weight 70 kDa, and DCl (99%D) were purchased from Sigma-Aldrich. NaCl (99.5%) was obtained from Fischer Scientific. All pH adjustments were performed using 1 M DCl and NaOH (Fischer Scientific). D_2O (99.8% D) used in the NR experiments was obtained from Acros. Ultrapure DI water with resistivity of 18.2 MΩ cm was used throughout our studies.

Single crystal 4 in. diameter quartz with a thickness of ∼10 mm was used as a substrate for LbL film deposition. Surface roughness of the quartz substrate was determined to be less than 5 Å rms using NR. The quartz substrates were rinsed with a chloroform and methanol solution, followed by cleaning with a piranha solution (H_2SO_4:H_2O_2, 3:1) for 6 h and subsequently rinsed with copious amounts of DI water. Finally, the substrates were exposed to UV radiation for 20 min.

2.2. Neutron Reflectometry. NR experiments were performed on the Surface Profile Analysis Reflectometer (SPEAR) beamline at the Los Alamos Lujan Neutron Scattering Center (LANSCE).[15] A pulsed neutron beam is produced from a spallation source and, after moderation by liquid H_2, is directed onto the sample at a very low angle while the specular reflection is recorded by a time-of-flight (ToF), position-sensitive detector. Reflectivity is defined as the ratio of the intensity of the reflected beam to the incident beam and is a function of the neutron momentum transfer vector Q_z, where $Q_z = 4\pi \sin(\theta)/\lambda$, θ is the angle of incidence of the beam, and λ is the wavelength of the neutron. Through analysis of the reflectivity vs Q_z data, the scattering length density (SLD) distribution normal to the sample surface and averaged over the beam footprint is obtained. SLD is a function of chemical composition and density of the material. Further details of NR measurements and modeling of the data have been detailed elsewhere.[15,16] The data presented here were analyzed by a model-dependent algorithm using the open-source MotoFit program.[17] The method optimizes the SLD profile describing the sample to obtain the best least-squares fit to the NR data. SLD is a value unique to a particular chemical composition and is the sum of

DOI: 10.1021/acs.langmuir.5b00037
Langmuir 2015, 31, 2870−2878

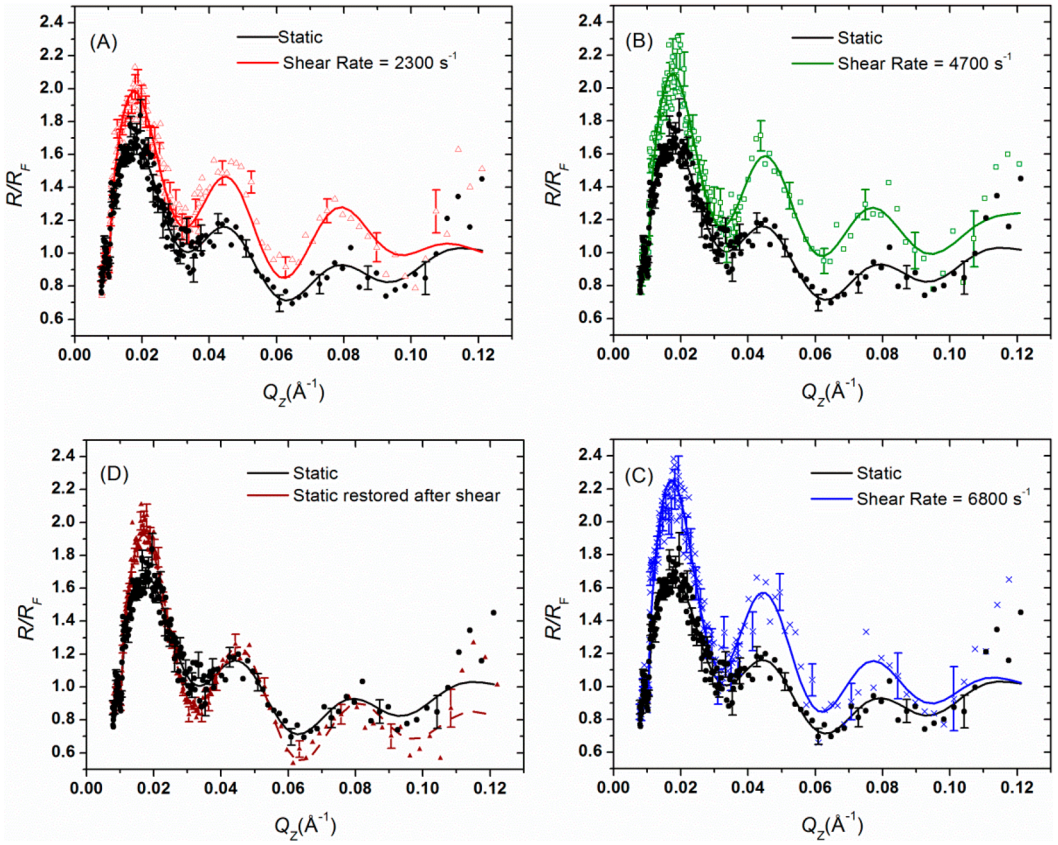

Figure 2. Fresnel normalized neutron reflectivity (R/R_F) of $[PEI\text{-}PSS]_4$-PEI measured at varying shear rates in pH 7 D_2O. Measured reflectivity at shear rates of 2300 s^{-1} (A), 4700 s^{-1} (B), and 6800 s^{-1} (C) and static condition restored after shear (D) are shown in comparison to the initially recorded reflectivity under static conditions (initial and restored after shearing). For normalization, reflectivity was divided by theoretically estimated Fresnel reflectivity for a quartz substrate in D_2O subphase.

the coherent scattering lengths of the constituent elements, divided by the volume they occupy. The SLD profile is shown as a function of distance from the interface in the direction normal to the sample surface. Model-dependent fitting is performed by comparing the NR profile to a model reflectivity profile generated using the Parratt recursion formalism[18] and adjusting the model using genetic optimization and the Levenberg–Marquardt nonlinear least-squares method to obtain the best least-squares fit. This approach is described as "box models" because the SLD distribution is described by a sequence of n boxes, each of constant SLD and thickness. Two adjoining layers i and $i + 1$ are connected by an error function centered at their interface to describe roughness between the layers. Roughness includes contributions from static roughness and dynamic undulations. We utilized the simplest possible model of physical relevance, the model with the fewest parameters, to describe the data.

A model-independent fitting approach based on B-spline profiles was also used. Model-independent fitting requires less *a priori* knowledge of the system as compared to model-dependent fitting. The result of model-independent fitting is a real-space interpretation of the NR data that is less biased by the experimenters' expectations of the SLD distribution. The SLD profile is composed of cubic or parametric B-splines.[19,20] Starting from an initial B-spline curve, a theoretical reflectivity profile is calculated and compared to the measured NR data. The B-spline curve is then modified, and the process is repeated until the corresponding theoretical reflectivity profile reproduces the measured NR data. The fitting procedure requires input of the following parameters: $\Delta\rho$, the difference in SLD of the substrate and subphase (in this case, quartz and deuterated subphase), n, the number of B-splines, d, the distance between the substrate and subphase, and β, a damping factor. Additional parameters employed to optimize computation include A_1, a function to determine the smoothness of the solution with a weight w_1; A_2, a biasing function to bias the solution toward an expected average SLD; and w_2, a second weight parameter to balance these two functions, A_1/A_2. Resulting SLD curves are refined by adjusting the parameters β, n, and d to obtain the best least-squares fit with physical relevance. While the output of the model-independent fitting procedure is a single SLD profile, the entire process was run iteratively over a range of input parameter values to produce over a thousand SLD profile solutions per data set. A subset of these solutions corresponding to the criteria $\chi^2 \leq \chi^2_{min} + 2$ was selected to best represent the sample's structure. The resulting SLD ribbons were smoothed for visual clarity. We found that the model-independent fits closely matched the model-dependent approach, giving us high confidence in the interpretation of the NR results.

2.3. PEI–PSS Multilayered Films. The polyelectrolyte films were deposited using the LbL technique, detailed elsewhere.[3,16,21] PEI and PSS solutions were prepared by dissolving 2 mg/mL of respective polyelectrolytes in DI water with 0.5 M NaCl. The pH values of PEI and PSS solutions were adjusted to 6 and 7, respectively. Deposition steps for each layer lasted for approximately 10 min followed by copious rinsing with DI water and drying under a N_2 stream each time. Following nine deposition steps, a sample with $[PEI\text{-}PSS]_4$-PEI architecture was obtained. The quartz substrate with $[PEI\text{-}PSS]_4$-PEI multilayered film was assembled within a flow cell as depicted in Figure 1, and the subphase was exchanged to D_2O. D_2O was used to increase the neutron scattering contrast between the hydrogenated PEM polymer layers and the liquid subphase.

3. RESULTS

For a fully developed flow between two parallel plates, the following expression is used to estimate the magnitude of the shear stress acting on each plate:

DOI: 10.1021/acs.langmuir.5b00037
Langmuir 2015, 31, 2870–2878

$$\tau = \mu\dot{\tau} = \mu\frac{6u_{av}}{h} \quad (1)$$

where τ is the shear stress [N/m^2 or Pa], $\dot{\tau}$ is shear rate [s^{-1}], μ is the viscosity [Pa·s], u_{av} is the average fluid velocity [m/s], and h is the height of the channel. By measuring the volumetric flow rate, we were able to calculate the average flow velocity. Subsequently, shear rate was estimated using eq 1. Note that this type of flow is also known as Poiseuille flow.

3.1. PEM Thin Film under the Liquid Flow Shear. In each case, before measuring the PEM layers in contact with liquid subphase, they were characterized by NR in air. Reflectivity profiles of PEM samples measured under different shear conditions are shown in Figure 2. Reflectivity data were divided by the calculated Fresnel reflectivity, R_F, of the quartz/D_2O interfaces and are displayed as R/R_F vs Q_z to compensate for the sharp decrease in reflectivity as described by Fresnel's law (i.e., $R \propto Q_z^{-4}$) and present the features of the data more clearly. Please note that Fresnel reflectivity was calculated for substrate/liquid interface assuming 5 Å roughness. A consistent and unidirectional change in the reflectivity profile with increasing shear rates is evident in Figure 2. Moreover, after returning to a static condition the reflectivity curve appeared to be similar (but not identical) to the initial static measurement. This implies that the effects of shear on PEM were partially reversible in the selected experimental conditions. The simplest and most physically reasonable model that fit the data for PEM under different shear conditions consisted of a two-box model. Our previous research on PEMs constructed from PEI and PSS reveal similar structures. However, in order to improve fits, especially in the high Q_z region of the NR, we modeled our data using a three-box model. The third box represents a small quantity of extremely hydrated polymer extending into the liquid subphase. It is possible that chains of polymer are dangling out of the PEM structure in a loosely packed form, and therefore, a third box was required to accommodate this region. The SLD profiles obtained from the three-box models are shown in Figure 3. In all cases, the SLD of quartz was set to 4.175×10^{-6} Å^{-2}, and the value of 6.3×10^{-6} Å^{-2} was used for D_2O subphase. Thickness and SLD values of each stratum have been listed in the tables included in the Supporting Information.

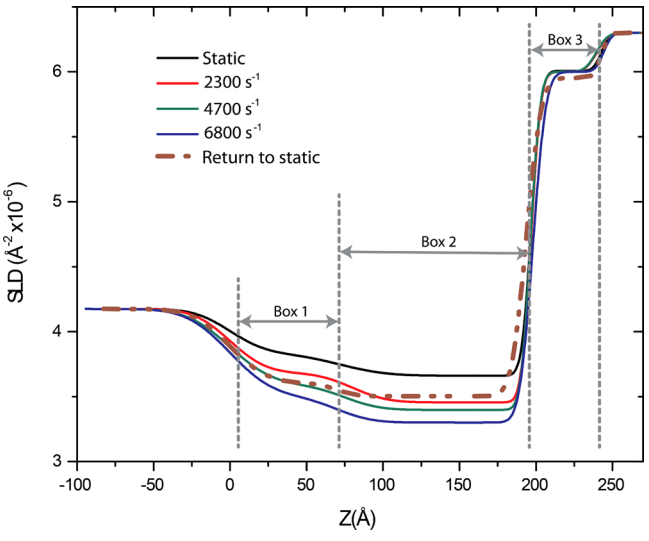

Figure 3. SLD profiles for [PEI-PSS]$_4$-PEI measured under varying shear rates at pH 7. SLD profiles correspond to the fits presented in Figure 2.

Figure 4 shows model-independent NR modeling of the pH 7 PEM data shown in Figure 2. The blue, red, and green ribbons represent the families of SLD profiles, which fulfill the criteria of $\chi^2_{min} + 2$ (where χ^2_{min} was approximately 10) for static, shear rate of 6800 s^{-1}, and restored static conditions, respectively. We also found that in the rest of the data discussed the SLD profiles resulting from the model-independent approach closely matched the SLD profiles obtained by model-dependent fitting.

NR measurements in air determined the SLD of the pure (dry) polymer layer to be 1.25×10^{-6} Å^{-2}, which matches the values from our previous work.[16] We used the following equation to estimate the hydration of each stratum for different shear conditions:

$$\alpha_w = \frac{(SLD^{box} - 1.25) \times 100}{6.3 - 1.25} \quad (2)$$

where α_w is the percentage hydration of a given stratum/box and SLD^{box} is the experimentally obtained SLD value of the respective stratum/box. Change in the hydration (α_w) of PEM with respect to shear rates is shown in Figure 5. The error bars represent the upper and lower bounds for hydration obtained by using SLD + standard deviation and SLD − standard deviation, respectively. Both SLD and standard deviations were obtained from the best fits shown in the tables (cf. Supporting Information). A consistent decrease in the hydration of box 1 and box 2 layers/strata can be noticed. However, the hydration of box 3, which mostly consisted of D_2O, remained constant as a function of shear and after return to static condition (i.e., no flow). After return to static conditions, the hydration of the bulk of the polymeric film increased relative to the highest shear rate case but was less than the original static measurement. Therefore, we can conclude that the hydration was only partially reversible, which is depicted in Figure 5. However, it is noted that the dehydration was limited (maximum ∼7%) and did not result in an observable difference in the thickness of the layers.

An important parameter determining the mechanical properties of a PEM is the polymer charge density.[22] For instance, if poly(acrylic acid) (PAA)/polyallyamine hydrochloride (PAH) multilayers are prepared at intermediate pH values where both polyelectrolytes are charged, the chains are more stretched and the Young's modulus (E) is high.[23] However, at lower pH, the chains are less charged, and therefore they should adopt a more coiled conformation and the E modulus is reduced to about 50% with respect to intermediate pH.[23] We should expect similar behavior in the case of PEM made of PEI/PSS although, since they are stronger polyelectrolytes, the effect should be significantly smaller. Therefore, to understand the role of charge density on the PEM constructed from PEI/PSS, we performed shear experiments at pH 3. The pH value of the D_2O subphase was lowered to ∼3 by adding a few drops of dilute DCl. The pK_a of PSS is ∼1; therefore, it will have a higher charge density at pH 7 compared to pH 3. Likewise, the pK_a of both primary and secondary amine groups in PEI is >10, and PEI will have a higher charge density at pH 7 in comparison to pH 3. Overall, we expect the polyions of our PEM to be more coiled and also exhibit lower E modulus at pH 3. NR and corresponding SLD profiles of the PEM measured in static conditions and under shear rate at pH 3 are shown in

DOI: 10.1021/acs.langmuir.5b00037
Langmuir 2015, 31, 2870−2878

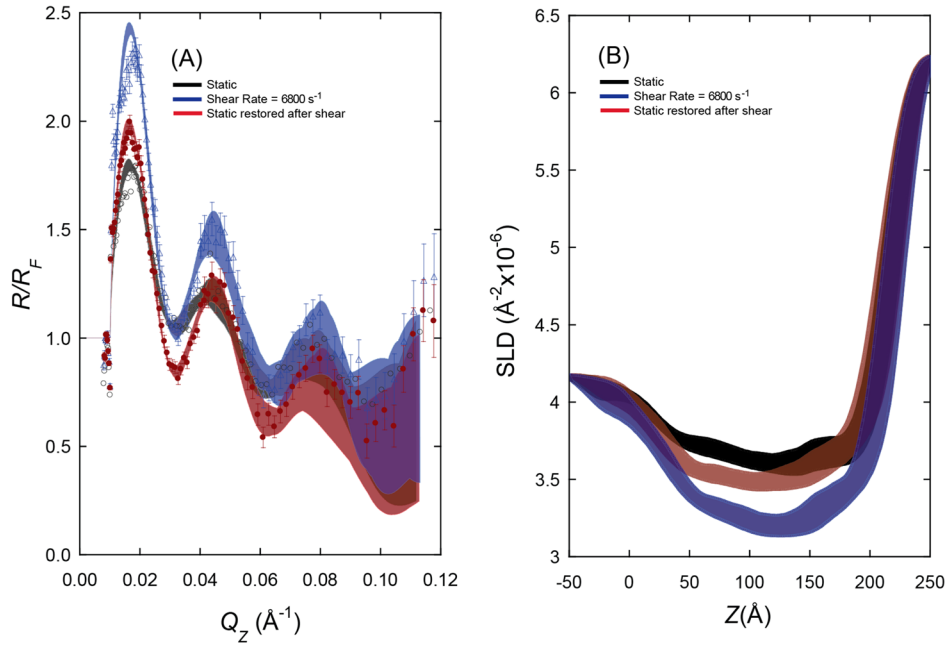

Figure 4. (A) Fresnel normalized neutron reflectivity (R/R_F) of $[PEI\text{-}PSS]_4$-PEI measured at varying shear rates in D_2O subphase at pH 7 and family of fits (shaded ribbons) obtained by the model-independent fitting approach described in the text. For each NR data the fitted curves are fulfilling the χ^2_{min} + 2 criteria. (B) Corresponding families of SLD profiles.

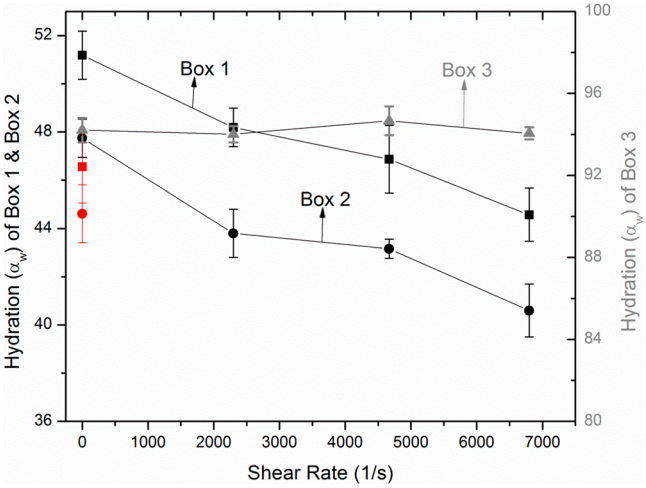

Figure 5. Hydration (α_w) of each stratum of PEM at pH 7 as a function of shear rate. Data in red denote the hydration values for respective strata upon the restoration of static condition. Note that box 3 mostly consisted of D_2O, and its hydration was almost constant.

Figure 6. Similar to the pH 7 case we observed changes in the NR profile when shear is applied. Also, the NR profile was found to be almost completely reversible upon the restoration of static condition. A corresponding decrease in SLD of the polymer is observed, which implies a reduced hydration of the PEM and, as in the case of pH 7, no significant changes in the overall thickness of the polymer. Using eq 1 and SLD values shown in Figure 6, we estimated the hydration of each layer/stratum of PEM, which is shown in Figure 7.

3.2. PNIPAAm Thin Film under the Liquid Flow Shear. The pNIPAM is a thermoresponsive polymer, which exhibits a volume phase transition at its lower critical solution temperature (LCST, 32 °C) and has been studied extensively since it was first reported 40 years ago.[24] Similarly to the PEM films, it is a highly hydrated polymer which, in response to small temperature variations, radically changes its volume by expanding and uptaking (below LCST) or collapsing and expelling (above LCST) water from its polymer chains. However, even in the "unhydrated form" approximately 50% of the film volume is occupied by H_2O molecules.[25−27] The detailed preparation method of pNIPAM film is described elsewhere.[25−27] Briefly, the pNIPAM was spin-coated onto a quartz substrate covered by a monolayer of 3-aminopropyltriethoxysilane. Interaction with the aminosilane allows the polymer to be tethered to the quartz surface. In our case the pNIPAM was copolymerized with 3 mol % of methacroylbenzophenone (MaBP) to form poly(NIPAM-MaBP). Addition of MaBP allows cross-linking of the polymeric network by exposure to UV light (365 nm) for 30 min. We compared the LbL deposited PEM films to the response of a poly(*N*-isopropylacrylamide) (pNIPAM) film exposed to the fluid shear stress. The pNIPAM film thickness was approximately half the thickness of the PEM films.

First we characterized the poly(NIPAM-MaBP) film in air and in contact with static D_2O below and above the LCST point (25 and 40 °C, respectively). In all cases we were able to model poly(NIPAM-MaBP) data by using one-box models. Figure 8 shows the reflectivity profile of poly(NIPAM-MaBP) film in air at 25 °C. This measurement allows estimating the thickness and the SLD of the film to be ∼114 Å and ∼1.1 × 10^{-6} $Å^{-2}$, respectively. Fresnel reflectivity was calculated for quartz/air interface assuming 5 Å roughness.

The poly(NIPAM-MaBP) film was subsequently measured in contact with D_2O. First, the static (no flow) experiment was performed at 40 °C when polymer was in a collapsed state (Figure 9). The NR experiments showed that the polymer film thickness, SLD, roughness, and hydration were 58 (±3) Å, 3.43 × 10^{-6} (±0.08) $Å^{-2}$, 4 (±0.3) Å, and 45.0%, respectively.

At shear rates less than 7000 s^{-1}, we were not able to observe any noticeable changes in the hydration of the polymer. Next,

DOI: 10.1021/acs.langmuir.5b00037
Langmuir 2015, 31, 2870−2878

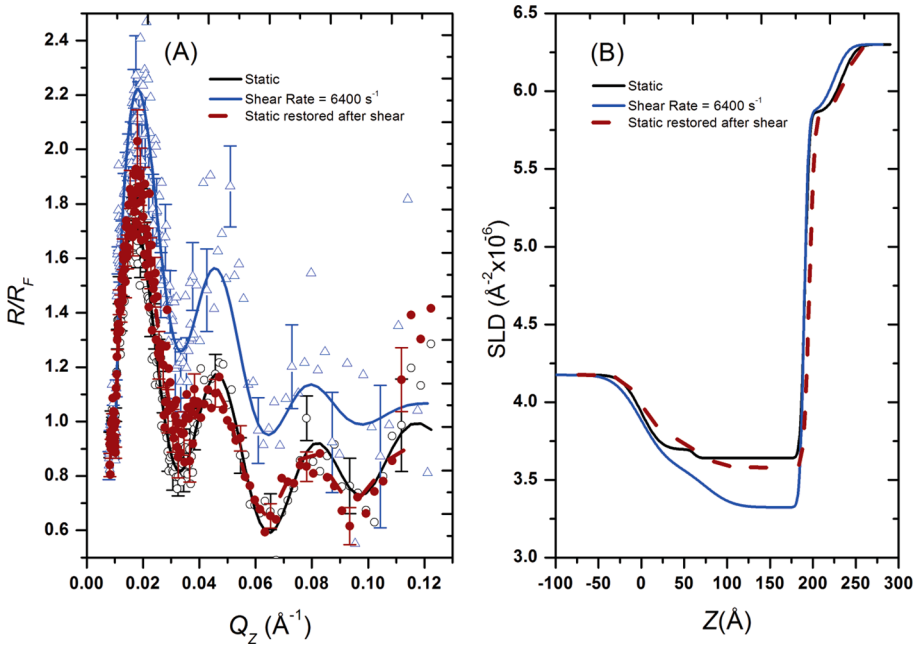

Figure 6. Fresnel normalized neutron reflectivity (R/R_F) of $[PEI\text{-}PSS]_4$-PEI measured at varying shear rates in D_2O subphase at pH 3 (A) and corresponding SLD profiles (B).

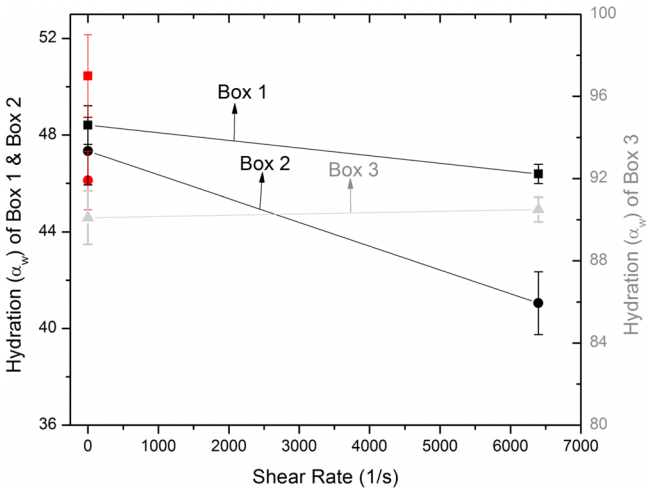

Figure 7. Hydration (α_w) of each stratum of PEM at pH 3 with respect to shear rates. Data in red denote the hydration values for respective stratum upon the restoration of static condition. Note that box 3 mostly constituted of D_2O, and its hydration was almost constant.

flow conditions were applied with a shear rate significantly higher (i.e., ~53 000 s^{-1}) than in our previous PEM experiments. The NR data indicated that the thickness, SLD, roughness, and hydration of the polymer film were 61 (±2) Å, 3.71×10^{-6} (±0.06) $Å^{-2}$, 6 (±0.4) Å, and 50.4%, respectively. The data (Figure 9) showed no significant change in the thickness of the polymer film, but only a small increase in the film roughness and its SLD values. The polymeric film returned to its original state after return to static conditions (Figure 9). The quartz roughness was fixed to 10 Å in all cases. It is to be noted that the surface modification of the quartz substrate in this case was performed using ethoxysilane layer, which resulted in slightly increased roughness.

We also measured the effect of shear when poly(NIPAM-MaBP) was in a swelled state (i.e., at 25 °C); however, no effect of shear was observed in this case (data not shown). Probably this is due to very high hydration of the polymer when it is in the swelled state and therefore much less favorable neutron scattering contrast conditions. The polymer can incorporate up to 90 vol % of water, and the SLD of the film cannot be easily distinguished from the subphase.

The NR data and the resulting SLD profiles indicated that at 40 °C the poly(NIPAM-MaBP) film in the flow shear stress conditions increased the water volume fraction by approximately 5% without any significant changes in the film thickness. It is an opposite effect than observed in PEM polymer presented before.

4. DISCUSSION

The osmotic pressure of water in an elastic, continuous polymer network can be divided into two parts:[28]

$$\Pi_{water} = \Pi_{mix} + \Pi_{elastic} \quad (3)$$

where the mixing term arises due to polymer−polymer contacts and the elastic term arises due to deformation of the polymer network. The mixing term depends on the volume fraction of polymer φ and an activity coefficient γ

$$\Pi_{mix} = -\frac{RT}{v} \ln[\gamma(1 - \varphi)] \quad (4)$$

where v is the molar volume of water. In good solvent conditions, the activity coefficient is between 0 and 1 (indicating that the polymer−water contacts are preferred over polymer−polymer contacts). In this case, the osmotic pressure due to mixing is always positive. It reaches a maximum as the polymer volume fraction approaches unity.

The elastic term is always negative and, depending on the model, can be a complicated function of ϕ; hence, we express the elastic term as

DOI: 10.1021/acs.langmuir.5b00037
Langmuir 2015, 31, 2870−2878

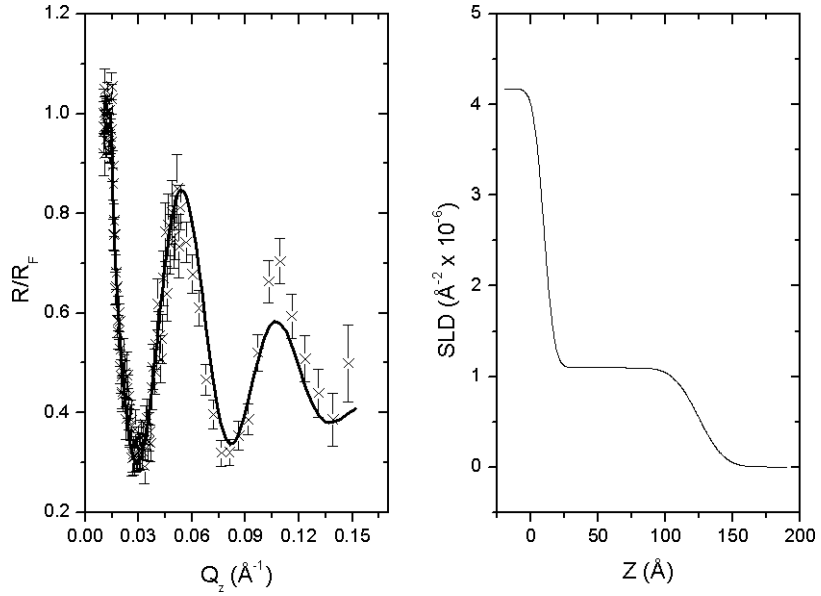

Figure 8. (A) Fresnel normalized NR of poly(NIPAM-MaBP) measured in air at room temperature. (B) SLD profile corresponding to the fit to the data.

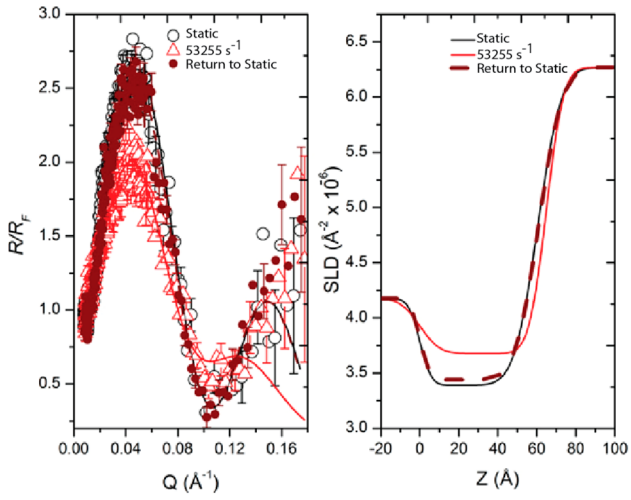

Figure 9. (A) Reflectivity and (B) SLD profiles of poly(NIPAM-MaBP) film with and without flow shear at 40 °C.

$$\Pi_{\text{elastic}} = -|f_{\text{elastic}}(\varphi)| \tag{5}$$

In the absence of flow, the following is true at equilibrium

$$\Pi_{\text{water}} = p_{\text{inside}} - p_{\text{outside}} \tag{6}$$

where $p_{\text{inside}} - p_{\text{outside}}$ is the static pressure difference between inside and outside of the network. To satisfy mechanical equilibrium, $p_{\text{inside}} = p_{\text{outside}}$ and hence $\Pi_{\text{water}} = 0$. Therefore, under conditions of no flow, the equilibrium swelling of the coating is determined when

$$\Pi_{\text{mix}} = \Pi_{\text{elastic}} \tag{7}$$

Now, in the case of flow, a Bernoulli energy balance relates the pressure inside and outside of the network:

$$P_{\text{inside}} - P_{\text{outside}} = +\frac{1}{2}\rho V_{\text{av}}^{\ 2} \tag{8}$$

where V_{av} represents the velocity external to the network relative to the velocity internal to the network. Hence, at equilibrium, and under flow, the equilibrium osmotic pressure of water in the network becomes positive.

$$\Pi_{\text{water}} = p_{\text{inside}} - p_{\text{outside}} = \frac{1}{2}\rho V_{\text{av}}^{\ 2} \tag{9}$$

Therefore, an incompressible network system will expand by taking up further solvent to satisfy the new equilibrium condition of

$$\Pi_{\text{mix}} > \Pi_{\text{elastic}} \tag{10}$$

This intuitively makes sense, as the network can be thought of as a semipermeable membrane. Reducing the external pressure allows the membrane to expand further.

Interestingly, no changes in the thickness are observed for either PEM or poly(NIPAAm-BP). In the case of poly(NIPAAm-BP), an increase in the flow rate leads to an increase in the density of the internal water. We hypothesize that water has a preferred structure and orientation inside the poly(NIPAAm-BP) network. If poly(NIPAAm-BP) expands at constant temperature, water can no longer have its preferred structure and may undergo pressure−volume work in that particular system.[29] This is based on the premise that water solvent molecules adjacent to solutes are known to be structurally and thermodynamically distinct from bulk water, which has been described by simple two-state models.[30] In these models, liquid water exists in a comprised state of both high density/high enthalpy and low density/low enthalpy species. Nevertheless, such models also fail to explain observed nonlinear volumetric changes commonly observed.[31]

The PEM, on the other hand, displays the opposite behavior, which may result from a different swelling mechanism. PEMs are strongly phase-segregated complex coacervates.[32] In this case, it is assumed that the activity coefficient is larger than one, meaning that polymer−polymer contacts are preferred over polymer−water contacts. Assuming a continuous water matrix within the PEM, the mixing osmotic pressure becomes negative with the uptake of water

$$\Pi_{\text{mix}} < 0 \tag{11}$$

DOI: 10.1021/acs.langmuir.5b00037
Langmuir 2015, 31, 2870−2878

To balance the negative osmotic pressure, there must also be a balancing positive osmotic pressure

$$\Pi_{water} = \Pi_{mix} + \Pi_{capillary} \quad (12)$$

which we attribute to capillary effects. The sign conventions dictates that water is driven into the PEM due to capillarity effects but is opposed by bulk mixing. Upon introduction of flow, eq 9 remains valid and now

$$\Pi_{mix} > \Pi_{capillary} \quad (13)$$

However, as the signs are reversed with respect to the previous case, the layer should contract with flow. Again, this intuitively makes sense, as a reduction of pressure external to the layer would pull capillary water from the PEM. As observed in the NR measurements, the layer does not contract, and hence water must adjust its density to accommodate the outflow of water.

5. CONCLUSION

The LbL deposited PEM film, deposited on quartz surface, were measured under different fluid shear stress conditions using NR. The fluid shear stress was applied through a laminar flow of liquid parallel to the quartz/polymer interface, i.e., in the Poiseuille geometry. It has been suggested that hydration of polymers can play a critical role in ascertaining the biocompatibility of such polymeric thin films.[33] Since hydration of polymeric coatings can vary with respect to fluidic shear, we believe that application of the described technique may be effective in studying biocompatible polymers under shear. The scattering length density profiles obtained from the NR results showed a monotonic decrease of the volume fraction of hydrating water with increasing shear rate. For the highest shear rate applied (6800 s^{-1}), the water volume fraction decreased by approximately 7% homogeneously throughout the film. The decrease in water content was not followed by any significant changes in the total polymer thickness, creating a negative osmotic pressure in the film. The PEM films were compared to the behavior of a thin film of thermoresponsive poly(*N*-isopropylacrylamide) (pNIPAM) approximately half the thickness of the PEM. At high shear rates the poly(NIPAM-MaBP) showed opposite behaviors under the fluid shear stress with the vol % of hydrating water increasing by approximately 5%. In both cases the polymers returned to their native states after the shear stress ended. The difference in the behavior of the two polymeric structures toward the fluid shear stress may arise from their different interactions with water molecules.

■ ASSOCIATED CONTENT

Ⓢ Supporting Information

Tables of fit parameters for PEM measured at pH 7 and 3 under different shear rates. This material is available free of charge via the Internet at http://pubs.acs.org.

■ AUTHOR INFORMATION

Corresponding Author

*E-mail jarek@lanl.gov (J.M.).

Notes

The authors declare no competing financial interest.

■ ACKNOWLEDGMENTS

This work benefited from the use of the Lujan Neutron Scattering Center at Los Alamos Neutron Science Center funded by the DOE Office of Basic Energy Sciences and Los Alamos National Laboratory under DOE Contract DE-AC52-06NA25396. We express special thanks to Flow Science, Inc., for providing the numerical flow simulation results and Dr. A. Zubelewicz (Los Alamos National Laboratory) for helpful discussions.

■ REFERENCES

(1) Ariga, K.; Hill, J. P.; Ji, Q. Layer-by-layer assembly as a versatile bottom-up nanofabrication technique for exploratory research and realistic application. *Phys. Chem. Chem. Phys.* **2007**, *9* (19), 2319−2340.

(2) Iler, R. K. Multilayers of colloidal particles. *J. Colloid Interface Sci.* **1966**, *21* (6), 569−594.

(3) Decher, G. Fuzzy nanoassemblies: Toward layered polymeric multicomposites. *Science* **1997**, *277* (5330), 1232−1237.

(4) Thevenot, P.; Hu, W.; Tang, L. Surface chemistry influences implant biocompatibility. *Curr. Top Med. Chem.* **2008**, *8* (4), 270−80.

(5) Park, J.; McShane, M. J. Dual-function nanofilm coatings with diffusion control and protein resistance. *ACS Appl. Mater. Interfaces* **2010**, *2* (4), 991−997.

(6) Qiu, Y.; Winterton, L. C.; Lally, J. M.; Matsuzawa, Y. Method for applying an LBL coating onto a medical device, 2005.

(7) Singh, S.; McShane, M. Role of porosity in tuning the response range of microsphere-based glucose sensors. *Biosens. Bioelctron.* **2011**, *26* (5), 2478−2483.

(8) Carlyle, W. C.; McClain, J. B.; Tzafriri, A. R.; Bailey, L.; Zani, B. G.; Markham, P. M.; Stanley, J. R. L.; Edelman, E. R. Enhanced drug delivery capabilities from stents coated with absorbable polymer and crystalline drug. *J. Controlled Release* **2012**, *162* (3), 561−567.

(9) Papaioannou, T. G.; Stefanadis, C. Vascular wall shear stress: Basic principles and methods. *Hell. J. Cardiol.* **2005**, *46*, 9−15.

(10) Prydal, J. I.; Artal, P.; Woon, H.; Campbell, F. W. Study of human precorneal tear film thickness and structure using laser interferometry. *Invest. Ophthalmol. Visual Sci.* **1992**, *33* (6), 2006−11.

(11) King-Smith, P. E.; Fink, B. A.; Fogt, N.; Nichols, K. K.; Hill, R. M.; Wilson, G. S. The thickness of the human precorneal tear film: Evidence from reflection spectra. *Invest. Ophthalmol. Visual Sci.* **2000**, *41* (11), 3348−3359.

(12) Heryudono, A.; Braun, R. J.; Driscoll, T. A.; Maki, K. L.; Cook, L. P.; King-Smith, P. E. Single-equation models for the tear film in a blink cycle: realistic lid motion. *Math. Med. Biol.* **2007**, *24* (4), 347−377.

(13) http://www.flow3d.com.

(14) Baker, S. M.; Smith, G.; Pynn, R.; Butler, P.; Hayter, J.; Hamilton, W.; Magid, L. Shear cell for the study of liquid-solid interfaces by neutron scattering. *Rev. Sci. Instrum.* **1994**, *65* (2), 412−416.

(15) Dubey, M.; Jablin, M.; Wang, P.; Mocko, M.; Majewski, J. SPEAR — ToF neutron reflectometer at the Los Alamos Neutron Science Center. *Eur. Phys. J. Plus* **2011**, *126* (11), 1−11.

(16) Singh, S.; Junghans, A.; Waltman, M. J.; Nagy, A.; Iyer, R.; Majewski, J. Neutron reflectometry characterization of PEI-PSS polyelectrolyte multilayers for cell culture. *Soft Matter* **2012**, *8* (45), 11484−11491.

(17) Nelson, A. Co-refinement of multiple-contrast neutron/X-ray reflectivity data using MOTOFIT. *J. Appl. Crystallogr.* **2006**, *39* (2), 273−276.

(18) Parratt, L. G. Surface studies of solids by total reflection of X-rays. *Phys. Rev.* **1954**, *95* (2), 359−369.

(19) Pedersen, J. S.; Hamley, I. W. Analysis of neutron and X-ray reflectivity data. II. Constrained least-squares methods. *J. Appl. Crystallogr.* **1994**, *27* (1), 36−49.

(20) Pedersen, J. S.; Hamley, I. W. In *Analysis of Neutron and X-ray Reflectivity Data by Constrained Least-Squares Methods*; Elsevier BV North-Holland: Amsterdam, 1994; pp 16−23.

DOI: 10.1021/acs.langmuir.5b00037
Langmuir 2015, 31, 2870−2878

(21) Singh, S.; Junghans, A.; Tian, J.; Dubey, M.; Gnanakaran, S.; Chlistunoff, J.; Majewski, J. Polyelectrolyte multilayers as a platform for pH-responsive lipid bilayers. *Soft Matter* **2013**, *9* (37), 8938−8948.
(22) Klitzing, R. Internal structure of polyelectrolyte multilayer assemblies. *Phys. Chem. Chem. Phys.* **2006**, *8* (43), 5012−5033.
(23) Pavoor, P. V.; Bellare, A.; Strom, A.; Yang, D.; Cohen, R. E. Mechanical characterization of polyelectrolyte multilayers using quasi-static nanoindentation. *Macromolecules* **2004**, *37* (13), 4865−4871.
(24) Heskins, M.; Guillet, J. E. Solution properties of poly(N-isopropylacrylamide). *J. Macromol. Sci., Chem.* **1968**, *2* (8), 1441−1455.
(25) Jablin, M. S.; Zhernenkov, M.; Toperverg, B. P.; Dubey, M.; Smith, H. L.; Vidyasagar, A.; Toomey, R.; Hurd, A. J.; Majewski, J. In-plane correlations in a polymer-supported lipid membrane measured by off-specular neutron scattering. *Phys. Rev. Lett.* **2011**, *106* (13), 138101.
(26) Smith, H. L.; Jablin, M. S.; Vidyasagar, A.; Saiz, J.; Watkins, E.; Toomey, R.; Hurd, A. J.; Majewski, J. Model lipid membranes on a tunable polymer cushion. *Phys. Rev. Lett.* **2009**, *102* (22), 228102.
(27) Vidyasagar, A.; Majewski, J.; Toomey, R. Temperature induced volume-phase transitions in surface-tethered poly(N-isopropylacrylamide) networks. *Macromolecules* **2008**, *41* (3), 919−924.
(28) Flory, P. J. *Principles of Polymer Chemistry*; Cornell University Press: Ithaca, NY, 1953.
(29) Chalikian, T. V. Structural thermodynamics of hydration. *J. Phys. Chem. B* **2001**, *105* (50), 12566−12578.
(30) Eisenberg, D.; Kauzmann, W. *The Structure and Properties of Water*, 1st ed.; Oxford University Press: New York, 1969.
(31) Chalikian, T. V. On the molecular origins of volumetric data. *J. Phys. Chem. B* **2008**, *112* (3), 911−917.
(32) Kizilay, E.; Kayitmazer, A. B.; Dubin, P. L. Complexation and coacervation of polyelectrolytes with oppositely charged colloids. *Adv. Colloid Interface Sci.* **2011**, *167* (1−2), 24−37.
(33) Chen, S.; Li, L.; Zhao, C.; Zheng, J. Surface hydration: Principles and applications toward low-fouling/nonfouling biomaterials. *Polymer* **2010**, *51* (23), 5283−5293.

DOI: 10.1021/acs.langmuir.5b00037
Langmuir 2015, 31, 2870−2878